Investigation of ion induced bending mechanism for nanostructures

Journal:	*Materials Research Express*
Manuscript ID:	MRX-101060.R1
Manuscript Type:	Paper
Date Submitted by the Author:	n/a
Complete List of Authors:	Rajput, Nitul; University of Strathcltyde, Department of Design, Manufacture and Engineering management Tong, Zhen; University of Strathclyde, Department of Design, Manufacture and Engineering management Luo, Xichun; University of Strathclyde, Department of Design, Manufacture and Engineering management
Article Keywords:	nanostructure manipulion, ion matter interaction, Si nanowire, focused ion beam (FIB)
Abstract:	Ion induced bending is a promising controlled technique for manipulating nanoscale structures. However, the underlying mechanism of the process is not well understood. In this letter, we report a detailed study of the bending mechanism of Si nanowires under Ga+ irradiation. The microstructural changes in the nanowire due to ion beam irradiation are studied and molecular dynamics simulations are used to explore the ion-nanowire interaction processes. The simulation results are compared with the microstructural studies of the nanowire. The investigations inform a generic understanding of the bending process in crystalline materials, which we suggest to be feasible as a versatile manipulation and integration technique in nanotechnology.

Investigation of ion induced bending mechanism for nanostructures

Nitul S Rajput[*], *Zhen Tong*[*] *and Xichun Luo*[*, §]

[*]Department of Design, Manufacture and Engineering management, University of Strathclyde, Glasgow G1 1XQ, United Kingdom

Abstract

Ion induced bending is a promising controlled technique for manipulating nanoscale structures. However, the underlying mechanism of the process is not well understood. In this letter, we report a detailed study of the bending mechanism of Si nanowires under Ga^+ irradiation. The microstructural changes in the nanowire due to ion beam irradiation are studied and molecular dynamics simulations are used to explore the ion-nanowire interaction processes. The simulation results are compared with the microstructural studies of the nanowire. The investigations inform a generic understanding of the bending process in crystalline materials, which we suggest to be feasible as a versatile manipulation and integration technique in nanotechnology.

KEYWORDS: nanostructure manipulation; ion matter interaction; Si nanowire; focused ion beam (FIB).

[§] Corresponding author: Prof. Xichun Luo, email: xichun.luo@strath.ac.uk; Tel: +44 141 574 5280

1. Introduction

In recent years, an interesting phenomenon of bending of nanostructures under bombardment by energetic ion beam has been observed. The phenomenon has been seen in several materials such as carbon and peptide nanotubes, amorphous carbon pillars, thin film structures, and metallic cantilevers [1-8]. In many cases, the bending process has been tried to understand on the basis of void-induced stress generation during ion beam irradiation [4, 5]. In some cases, the phenomenon is attributed to ion induced thermal stress as discussed in ref. [2, 3]. In others, the bending process is thought to result from volumetric expansion caused by ion implantation. Depending on the energy of ion beam and the length scale of ion implantation the nanowire bends towards and away from the ion beam [6-8]. But in general the underlying physics of the phenomenon is not clear. Nonetheless, the process has been successfully used to fabricate tailored three-dimensional structures and to create nano-mechanical devices [3, 5, 9-11]. These studies suggest that the process can be potentially used as a manipulation and nanointegration technique in nanotechnology, for which an in-depth understanding of the underlying process is necessary.

In this paper, we present detailed investigations of the ion induced bending (IIB) of Si nanowires (NWs). The NWs are fabricated using the top-down process of focused ion beam (FIB) milling. Si NWs are chosen in particular as they are promising building blocks for next generation nano scale devices [12-15]. We find that the fabricated NWs move and modify their shapes during the course of irradiation until it reaches a stable configuration. This IIB process of the NWs is found to be precise and highly controllable.

In order to understand IIB, an atomistic investigation in terms of ion-nanowire interaction (i.e. damage formation and reorganization of the atomic layers) has been carried out. Microstructural investigations of the NWs indicate that reorganization within the ion induced damage layers triggers the bending process. Further, we use molecular dynamics simulations to understand the ion induced atomistic processes and inform our interpretation of the experimental data.

2. Experimental details

A (111)-oriented Si wafer was used as the base material for NW fabrication. Ion milling and irradiation were performed using an FEI Nova 200 Dualbeam FIB system that is equipped with an Omniprobe 100 micromanipulator and two gas injection systems for transmission electron microscopy (TEM) sample preparation [16]. Typically, a 30 keV, 0.48 nA Ga^+ beam was used to remove material selectively from the Si substrate to fabricate micron wires. Hollow cylindrical trenches were fabricated using the FIB milling to create the wires. Circular patterns having outer diameters 10-15 μm and inner diameters of 2-3 μm were employed to fabricate the cylindrical trenches. The process leaves the inner side as a micron wire standing perpendicular to the substrate. Maximum focusing of the Ga^+ beam in conventional FIB systems is usually obtained at high beam voltage with low beam current. Therefore, the beam current was decreased to 9.7-48 pA and selectively irradiated on the sides of the fabricated micron wires from a tilted angle to thin down the wires further. Using this approach, fine NWs of diameters as low as 25 nm can be fabricated. A scanning electron microscopy (SEM) image of a 50-nm-diameter NW is shown in Figure 1(a).

3. Results and discussion

3.1. Bending of Nanowires

3.1.1. Observation. The fabricated NW was subsequently irradiated from the angle indicated by the arrows at the top of the images in Figure 1. At this stage, the beam voltage and the current were 16 kV and 21 pA, respectively. The initial arbitrary irradiation angle on the NW was 36° (Figure 1(a)). We find that the wire tends to bend towards the ion beam direction as indicated in the sequence of images, Figures 1(a) to 1(c). During the course of bending, the NW tends to form a curved shape. Gradually, orientation of the upper portion of the NW becomes parallel to the ion beam and eventually bends away from the ion beam. At this stage, the opposite surface of the wire starts receiving the irradiation (Figure 1(d)) and starts bending in the reverse direction (Figure 1(d)-(f)). Gradually, the shape of the wire changes from the initially curved shape to align straight along the beam direction and finally equilibrates lying parallel to the ion beam direction.

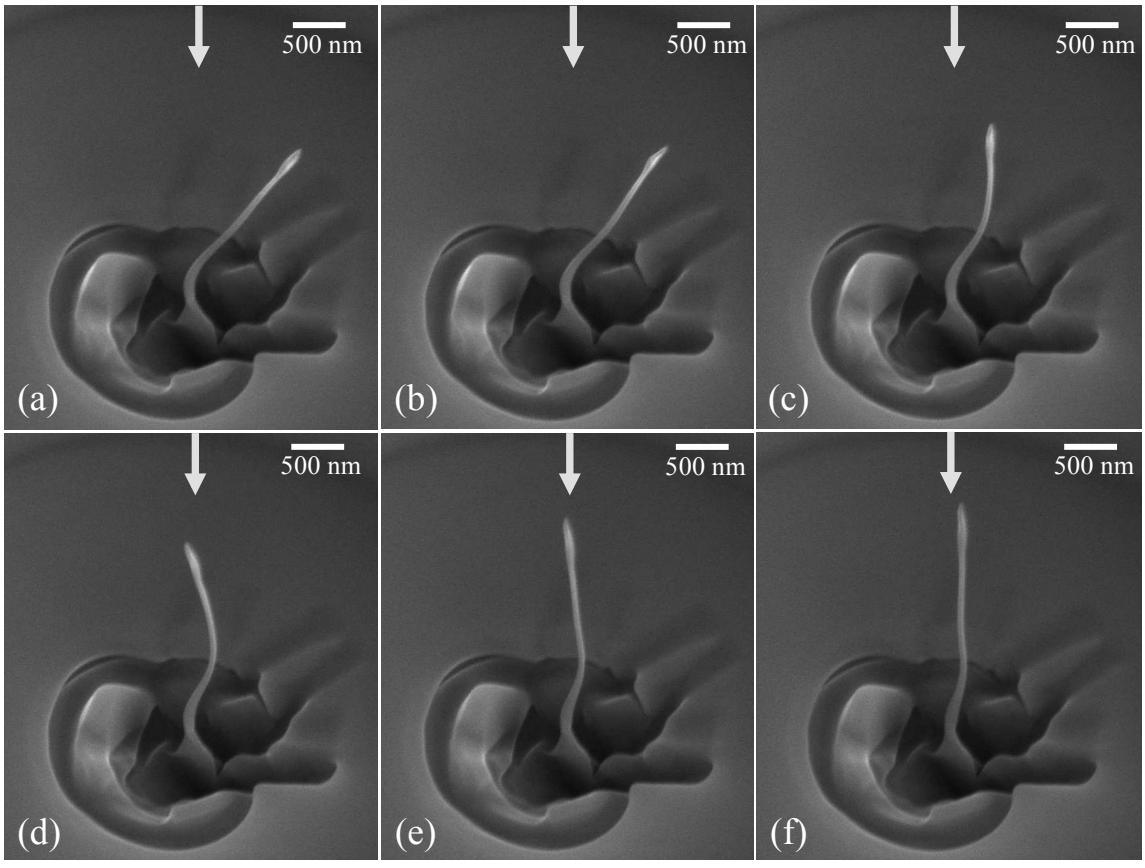

Figure 1. SEM snapshots taken at different stages during the bending of a Si NW. The arrows represent the incident ion beam direction. The initial irradiation angle was 36°. Applied beam voltage and current were 16 kV and 21 pA. The ion beam doses used to achieve the bending shapes were: (b) 0.33 × 10^6 ions μm^{-2}, (c) 1.65 × 10^6 ions μm^{-2}, (d) 3.31 × 10^6 ions μm^{-2}, (e) 5.0 × 10^6 ions μm^{-2}, and (f) 6.66 × 10^6 ions μm^{-2}.

The minimum dwell time that can be set in the SEM imaging process is 50 ns and within this observation scale (image acquisition time ~ 0.05 s), the bending process appears instantaneous and the deformation is plastic i.e., the wire remains bent and stationary once the ion beam is switched off. The shape evolution of the NW during the bending process is shown by the false-colored montage in Figure 2(a). Since the shape of the NW is not initially a uniform curve, we quantify the deflection by drawing a line that connects the tip of the wire to the center of the wire. The angle made by this line with the ion beam direction is taken as the bending angle of the NW (Figure 2(b)). A graphical representation of the bending pattern is shown in Figure 2(c), which plots the variation of the bending angle of the NW with the ion beam fluence.

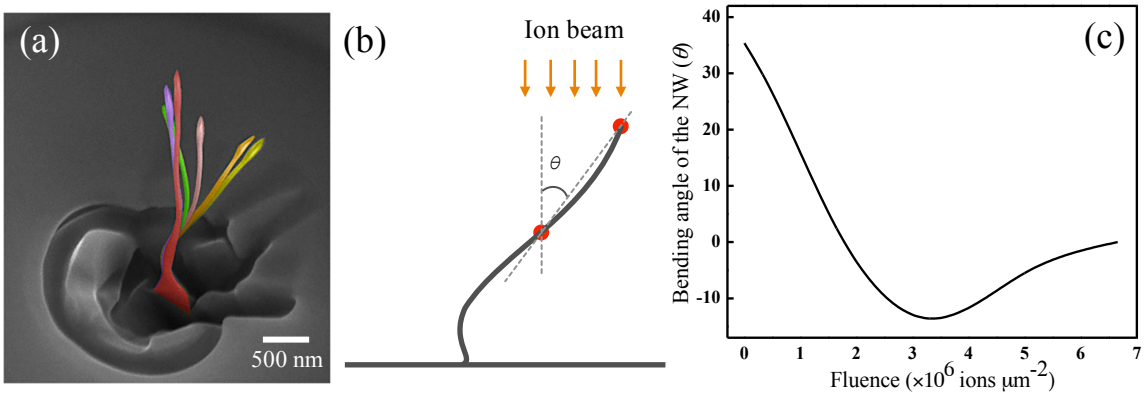

Figure 2. (a) A false-colored overlapped image showing the bending evolution of the NW. Color representation: (a) yellowgreen, (b) orange, (c) pink, (d) springgreen, (e) violet, and (f)

indianred. (b) Schematic diagram shows the bending angle θ. (c) The graphical representation of the bending pattern of the NW (bending angle vs. ion beam fluence).

3.1.2. Bending Mechanism. In order to understand this nanoscale phenomenon, an atomic scale understanding of the ion-nanowire interaction process is important. When an energetic ion particle enters into the solid, it transfers its energy and momentum to the target atoms and creates voids and interstitials in addition to surface sputtering. A variety of defects can be formed and the amount depends on the sample material, incident beam type, irradiation parameters, etc. [17]. When the 16 keV Ga^+ ions enter into the nanoscale material (Si NW), they remove atoms from the surface layers of the NW, produce different amount of voids at different depths and ultimately induce recrystallization in the NW [17, 18]. As a result of the atoms removal (sputtering) and rearrangement of the disturbed atoms a compressive stress is expected to be built up at the front facing layers. It is seen that through the defect formation and recombination process of the defects, ion beam can produce significant amount of stress of GPa order on a sample surface [19, 20]. This provides a simple mechanism for the bending of the NWs in the present case. If the outer most layers facing the ion beam irradiation shrink as a result of the developed compressive stress, this will affect the nearest connected layers as well and induce a deformation in the system. As a result, a new equilibrium shape is achieved with the NW bending towards the ion beam side.

The bending of the NW continues (till Figure 1(c)), after which the opposite surface of the NW starts receiving the irradiation (Figure 1(d)) and as a result, the NW starts bending back towards the ion beam (Figure 1(d)-(f)). During this course of bending, the front face of the lower part of the NW is again exposed to the irradiation and this will cause the NW to bend in the opposite direction than that of the upper part of the NW. The competition between these two opposite

bending directions enforces the NW to take a straight shape nearly parallel to the ion beam direction. During the bending process, reduction in the wire thickness or the wire height due to sputtering process is not specifically observed, which suggest of low sputtering rate as compared to high bending rate of the NW. However, as soon as the wire aligns with the ion beam, the height gradually reduces with the beam dose. This is in accordance with the experimental observation that a single NW can be bent many times back and forth (by changing the ion beam direction) without drastically damaging the NW. The observation also informs about the reversible nature of the IIB phenomenon. A scanning ion microscope (SIM) video showing the bending of a Si NW under 16 keV Ga ion beam irradiation is available online (supplementary information, Movie S1).

3.1.3 Microstructural Studies. TEM investigations were carried out on the NWs to study the structural modifications during the bending process. An FEI Tecnai T20 instrument equipped with a Gatan Imaging Filter for elemental analysis was used to study the chemical modifications of the NW. For this work, nanowires were fabricated from a portion of Si that had been welded to a Cu TEM grid using the in-situ micromanipulator and a standard FIB lift-out technique [16]. This approach was found to be more reliable than fabricating the wires prior to lift-out. TEM results obtained from freshly prepared NWs (without bending process) suggest that due to ion beam irradiation the prepared NWs become polycrystalline during the fabrication process (supplementary information, Figure S1). In order to see the atomic modifications of such a NW due to the IIB process, a Si NW is prepared and bent multiple times. A bright field TEM image of the Si NW that had previously been bent multiple times is shown in Figure 3(a). The diameter of the NW is 35 nm. Both the patchy contrast in the main image and rings of diffraction spots in the inset image indicate the nanowire to be polycrystalline. This structure is more obvious in the

higher-resolution image shown in Figure 3(b), which shows the presence of several crystalline planes at random orientations with respect to the NW axis (and thereby the Si substrate). A thin amorphous shell of non-uniform thickness is also evident. The amorphous shell may have grown during the TEM imaging due to the presence of organic contamination since we found that excessive e-beam irradiation during TEM imaging led to the growth of thick amorphous layers on some part of the NW (supplementary information, Figure S2).

The TEM studies clearly indicate that even after multiple bending of the NW the structure is not completely amorphized by the ion beam irradiation and it retains its polycrystalline nature, which indicates the presence of a strong recrystallization tendency in the damaged Si layers.

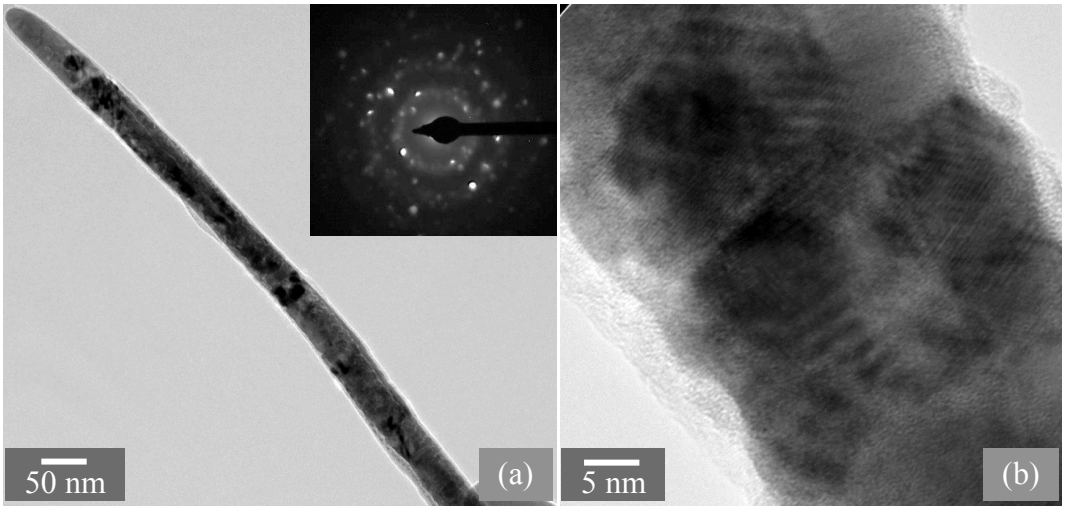

Figure 3. (a) A bright field TEM image of a typical Si NW after multiple bending experiments. The inset shows a convergent beam electron diffraction pattern collected from the NW. (b) A higher magnification image of the NW, revealing the presence of anamorphous shell of variable thickness and a polycrystalline core.

3.1.4 Molecular Dynamics Simulation. To achieve in-depth understanding of the atomic-scale mechanisms driving the IIB process, we have performed molecular dynamics (MD) simulations.

A model was built to study the bombardment process of a single crystal Si NW (diameter 21.7 nm) by 16 keV Ga^+ ions. The three orientations of the workpiece ([1 0 0], [0 1 0], and [0 0 1] along the X, Y, and Z directions) are shown in Figure 4(a). In order to model heat dissipation during the ion collision process, two thermal layers were built at each end of the NW (Figure 4(b)). A combination of the Tersoff and ZBL potential was used for the simulation [21-23]. At the beginning of each ion collision, Ga ions were introduced at a random location above the irradiation area (defined as 2.5 nm × 2.5 nm) as shown in Figure 4(b). The incidence angle of the Ga ions with respect to the NW (Z-axis) was 36°, equivalent to the initial incidence angle (θ) used in our experiment (Figure 1). The simulation time step was kept at 0.1 fs and an interval time of 140 ps was employed for the workpiece to cool down to 293 K for each single ion collision. The concept of atomistic equivalent temperature [24] was employed to analyze the temperature distribution at the core collision area (indicated by the dotted line in figure 4 (b)). Figure 4(c) shows the damage zone across the NW after the irradiation of ion fluence of 4×10^6 ions μm^{-2} and subsequent cooling. The recrystallized zones are shown by the hexagonal marks and the atoms in violet color represent the residual defects after the collision process. If longer simulation times were used then these residual defect zones are expected to form grain boundaries separating the crystalline zones [18]. Hence, these simulation results can be closely compared with the corresponding experimental data obtained from TEM image (Figure 3).

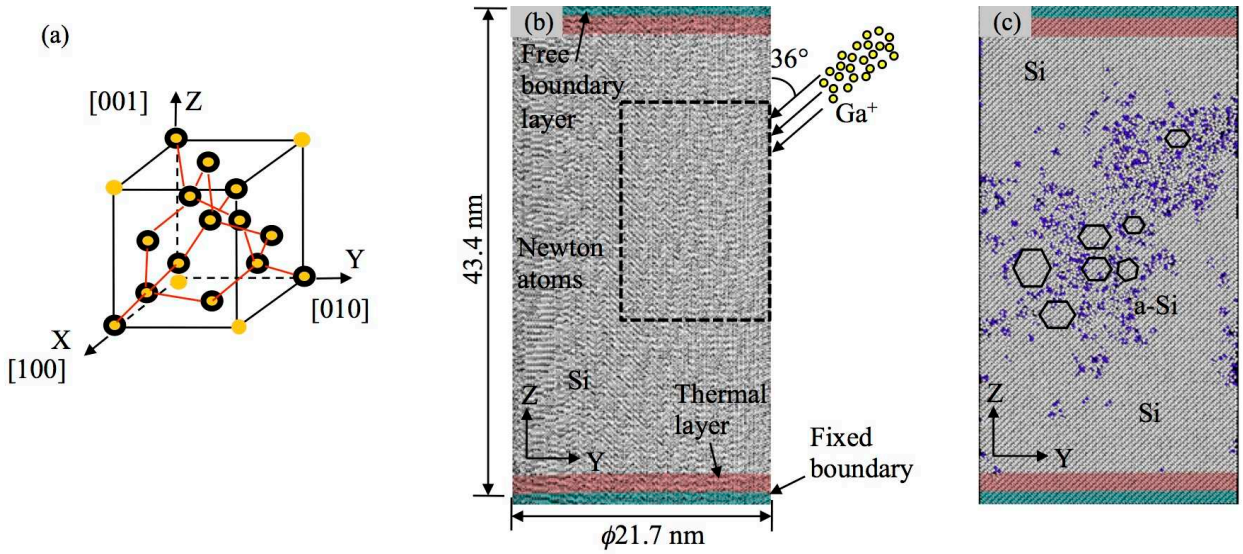

Figure 4. Multi-particle Ga^+ collision MD simulation model. (a) The diamond crystalline lattice and the corresponding coordinate axes. (b) The dimensions of the Si NW model (front view) with incidence angle of the Ga ions of 36°. (c) A cross-sectional view of the NW after the irradiation of ion fluence of 4×10^6 ions μm^{-2} (16 keV Ga^+) and subsequent cooling down to 293 K. The violet atoms refer to the atomic defects inside the Si NW. The dotted line in figure 4 (b) indicates the core collision area selected for temperature analysis. The hexagonal marks indicate the recrystallized zones within the collision cascade region.

The local temperature and the collision-dynamics during the interaction of a single 16 keV ion with the Si NW are shown in Figure 5. Each Si atom was colored by the atom's common neighbor value [25]. Defect-free regions (Si atoms of perfect diamond structure) were removed from the visualizations. As shown in Figure 5, the single ion collision process comprises a temperature spike portion (encircled by the dotted line in Figure 5; magnified and shown in inset (a)) and a relatively long stage of recrystallization process (discussed below).

Initially, the irradiated Ga ion interacts with the Si atoms and a large number of atomic damages

(vacancies and interstitials) are created (inset (b) in Figure 5). During this period, the Ga ion transfers its kinetic energy partly into thermal energy to the target material. At 0.054 ps, the local temperature reaches a peak value of 1254.4 K (T_p). This highest local temperature region is located at the surface facing the ion beam irradiation as shown by the encircled line in inset (b), Figure 5. Surface sputtering was also observed after T_p (inset (c) in Figure 5). The average sputtering of Si atoms observed during the simulation was 5. Also, the damage zone was observed to grow continuously through the displacement cascades. The peak disorder of the local lattice structure was found at 0.26 ps at which the local temperature was 663 K (inset (d) in Figure 5). Following the growth of the damage zone, there is a long stage of relaxation, during which the local high temperature provides thermal energy to the atomic defects to anneal back to diamond structure [18, 26]. After the full-relaxation-process, it is seen that more than half of the defects are annealed back to diamond crystal structure, and only a few atomic defects remain in the Si sample (inset (e) in Figure 5).

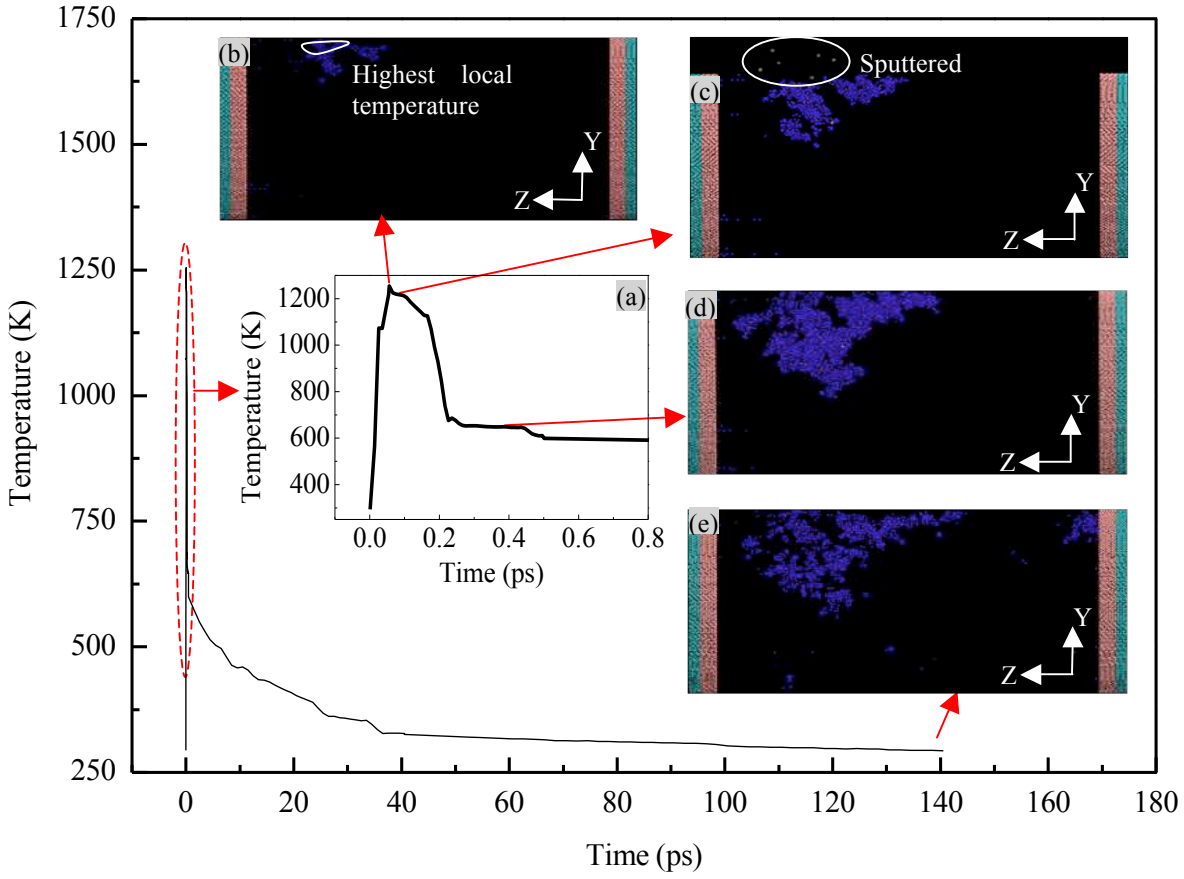

Figure 5. Molecular dynamics simulations describing the temperature evolution and the recrystallization process for the first single ion collision. Inset (a): the local view of the temperature during the temperature spike phase. Inset (b): the initial defects created when the local temperature has reached the peak value of 1254.4 K at 0.054 ps; this highest temperature region is shown by the encircled line. Inset (c): an intermediate phase during the defect formation process observed at 0.092 ps; surface sputtering is also observed at this stage. Inset (d): the defect configuration at the stage of the peak disorder of the lattice achieved at 0.26 ps. Inset (e): the residual defects after the system is cooled down to 293 K at 140 ps. The Si atoms of perfect diamond structure are removed from the visualizations.

The stress developed due to the damage formation and recrystallization processes may depend on

various parameters [19, 27]. In order to look into the dynamic process of the stress development in the nanowire due to ion beam irradiation, the atomic stress was calculated from the simulation data using viral stress theorem [28, 29]. It is observed that under the irradiation dose of 4×10^6 ions μm^{-2} (with the same irradiation geometry as used before, Figure 4(b)), the stress developed during the time of damage evolution (at 0.34 ps) is positive at the region facing the irradiation (shown by the elliptical dotted line in Figure 6) and the stress at the opposite zone of the NW (shown by the rectangular dotted line in Figure 6) is negative. It is seen that the stress distribution across the NW changes with time. Figure 6(b) is the stress distribution profile across the NW at an intermediate stage of 0.50 ps. Figure 6(c) shows the distribution of stress across the NW at 140 ps, i.e., after the long stage of recrystallization process. At this stage, the stress at the region facing the ion beam irradiation becomes negative (compressive) and the stress at the opposite zone of the NW becomes positive (tensile) (Figure 6(c); shown by the elliptical and the rectangular dotted lines respectively). The difference in the stress distribution across the NW, which is of the order of GPa, is the anticipated driving force for the mechanical deformation of the NW, which eventually appears as bending of the NW towards the irradiation side.

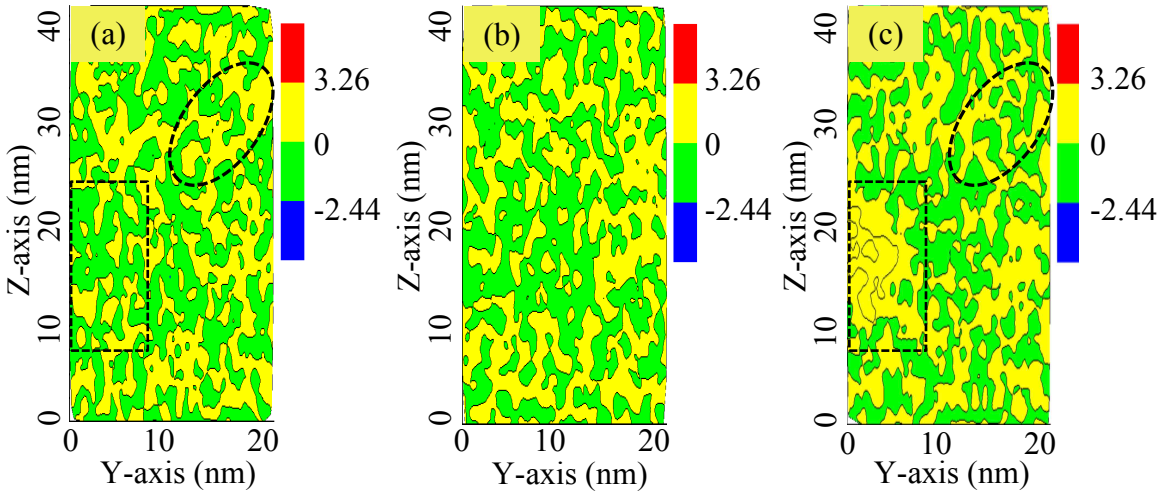

Figure 6. Stress development in the NW due to ion beam irradiation. The Ga ions fell on the NW making an angle of 36^0 with respect to Z-axis (Figure 4(b)). (a) Shows the distribution of stress at time 0.34 ps, (b) is the distribution at time 0.50 ps and (c) is the stress distribution at time 140 ps. In all the cases, the unit of the stress is in GPa.

Thus, the results obtained from the MD simulations can be efficiently used to understand the ion-NW interaction and the NW bending process.

3.2. Nanowire Characterization. Further, we characterize the NWs fabricated by the ion beam milling process. A bright field TEM image of a freshly prepared Si NW (25 nm diameter) is shown in Figure 7. The image shows large number of black spots, roughly in spherical shape and distributed throughout the wire that are consistent with mass-thickness and diffractive contrast variations. Elemental mapping of the NW (corresponding to the dotted portion shown in the image) is shown in the insets (b) and (c) in Figure 7, where insets (b) and (c) are energy filtered TEM (EF-TEM) images of Ga and Si elements, respectively. The EF-TEM images indicate that the black spots are Ga enriched regions (GaERs), suggesting that the implanted Ga ions do not remain uniformly dissolved in the Si matrix but segregates into strongly enriched particles, in agreement with earlier studies [30]. The thermal environment created by the irradiation may assist in the diffusion of Ga ions within the collision-cascade regions. In our present experimental conditions, no blistering or nanodot formation on the surface of the NWs is observed. However, the dynamics of the agglomeration process of the Ga ions to form GaERs in the NWs might have the similar mechanism. The approximate size distribution of the GaERs

with the Lorentzian fit is shown in the inset of the image (inset (d)), which shows the dominance of GaERs with size 3-5 nm.

A close inspection on the image, inset (c) in Figure 7 reveals that the tip of the NW is partly deformed. The deformation is likely to be caused by the excessive e-beam irradiation during the TEM imaging. This enlightens the interesting aspect of NW bending: the role of thermal energy in IIB process. The energetic electrons can produce heat in the NW material while passing through the wire and this can provide thermal energy to the NW for further recrystallization and subsequent shape-modification of the NW.

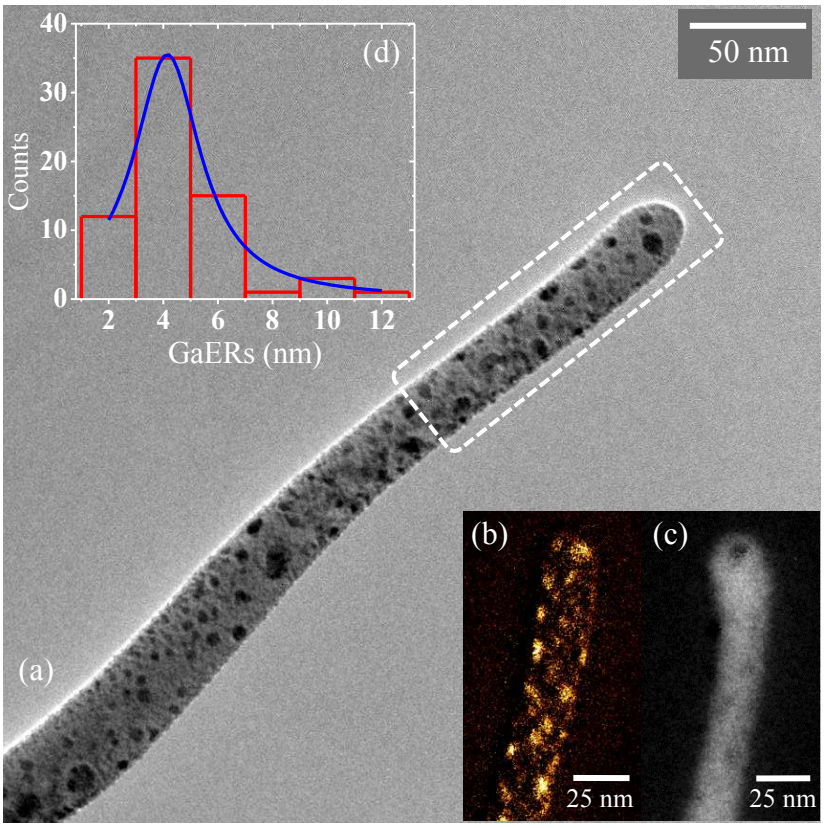

Figure 7: (a) A bright field TEM image of a Si NW taken immediately after fabrication. Elemental mapping of the wire (insets (b) and (c)) corresponding to the dotted portion in the

bright field image indicates that the dark features observed in the bright field imaging are Ga enriched (inset (b)). Inset (c) is an EF-TEM image of Si. The approximate size distribution of the Ga enriched regions (GaERs) is shown in the inset (d). The Lorentzian fit is shown by the solid blue line in the graph (inset (d)).

4. Conclusion

In summary, we have discussed the underlying mechanism of ion-induced bending of crystalline Si NWs. The results of microstructural study and molecular dynamics simulation support the hypothesis of ion induced amorphization, recrystallization and subsequent formation of plastic strain, which in turn triggers the bending process. The studies show the generic nature of the bending process for nanoscale crystalline materials and opens up the possibility of using the phenomenon as a versatile manipulation and integration technique in the future.

Acknowledgements

We acknowledge the financial support from EPSRC (EP/K018345/1), UK. We thank W. Smith and C. How of the University of Glasgow for assistance with FIB and TEM measurements, respectively and are grateful for discussions with D. A. MacLaren.

REFERENCES

(1) Park B. C.; Jung K. Y.; Song W. Y.; O B.; Ahn S. *J. Adv. Mater.* **2006**, 18, 95.

(2) Gour N.; Verma S. *Soft Matter* **2009**, 5, 1789.

(3) Tripathi S. K.; Shukla N.; Dhamodaran S.; Kulkarni V. N. *Nanotechnology* **2008**, 19, 205302.

(4) Yoshida T.; Nagao M.; Kanemaru S. *Jpn J. Appl. Phys.* **2010**, 49, 056501.

(5) Rajput N. S.; Banerjee A.; Verma H. C. *Nanotechnology* **2011**, 22, 485302.

(6) Borschel C.; Spindler S; Lerose D.; Bochmann A.; Christiansen S. H; Nietzsche S.; Oertel M.; Ronning C. *Nanotechnology* **2011**, 22, 185307.

(7) Borschel C.; Niepelt R.; Geburt S.; Gutsche C.; Regolin I.; Prost W.; Tegude F.; Stichtenoth D.; Schwen D.; Ronning C. *Small* **2009**, 5, 2576.

(8) Pecora E. F.; Irrera A.; Priolo F.; *Physica E* **2012**, 44, 1074.

(9) Chalapat K.; Chekurov N.; Jiang H.; Li J.; Parviz B.; Paraoanu G. S. *Adv. Mater.* **2013**, 25, 91.

(10) Yoshida T.; Nishi T.; Nagao M.; Shimizu T.; Kanemaru S. *J. Vac. Sci. Technol. B* **2011,** 29, 032205.

(11) Tripathi S. K.; Shukla N.; Rajput N. S.; Dhamodaran S.; Kulkarni V. N. *Micro & Nano Letters* **2010**, 5, 125.

(12) Li Y.; Qian F.; Xiang J.; Lieber C. M. *Mater. Today* **2006**, 9, 18.

(13) Choi S.; Ahn J.; Han J.; Seol M.; Moon D.; Kim S.; Choi Y. *Nano Lett.* **2011**, 11, 854.

(14) Cui Y.; Lieber C. M. *Science* **2001**, 291, 851.

(15) Chen L. J. *J. Mater. Chem.* **2007**, 17, 4639.

(16) Ke X.; Bals S.; Negreira A. R.; Hantschel T.; Bender H.; Tendeloo G. V. *Ultramicroscopy* **2009**, 109, 1353.

(17) Yao N. *Focused Ion Beam Systems: Basics and Applications*, Cambridge University Press, New York, 2007.

(18) Pelaz L.; Marques L. A.; Barbolla J. *J. Appl. Phys.* 2004, 96, 5947.

(19) Medhekar N. V.; Chan W. L.; V B Shenoy V. B.; Chason E. *J. Phys.: Condens. Matter* **2009**, 21, 224021.

(20) Madi C. S; Davidovitch B.; George H. B.; Norris S. A.; Brenner M. P.; Aziz M. J. *Phys. Rev. Lett.* **2008**, 101, 246102.

(21) Tersoff J. *Phys. Rev. B* **1988,** 37, 6991.

(22) Ziegler J. F.; Biersack J. P.; Littmark U. *The Stopping and Ranges of Ions in Matter*, Pergamon Press, New York, 1985.

(23) Satake S.; Ono K.; Shibahara M.; Taniguchi J. *Nucl. Instr. Meth. Phys. Res. B*, **2013**, 307, 235.

(24) Tong Z.; Liang Y.C.; Yang X.C; Luo X.; *Int J Adv Manuf Technol.* **2014**, 74, 1709.

(25) Tsuzuki H.; Branicio P. S.; Rino J. P. *Comput*. *Phys*. *Commun*. **2007**, 177, 518.

(26) Borodin V. A. *Nucl. Instr. Meth. Phys. Res. B*, **2012**, 282, 33.

(27) Chan W.; Zhao K.; Vo N.; Ashkenazy Y.; Cahill D. G.; Averback R. S. *Phys. Rev. B* **2008**, 77, 205405.

(28) Subramaniyan A. K.; Sun C. T. *Int. J. Solids Struct.* **2008**, 45, 4340.

(29) Zhou M. *Proc. R. Soc. Lond. A* **2003,** 459, 2347.

(30) Buckmaster R.; Hanada T.; Kawazoe Y.; Cho M.; Yao T.; Urushihara N.; Yamamoto A. *Nano Lett.* **2005**, 5(4), 771.